Research paper

New amidine-benzenesulfonamides as iNOS inhibitors for the therapy of the triple negative breast cancer

Q6

Q5

The corrections made in this section will be reviewed and approved by a journal production editor.

M. Dora Carrión[a], Belén Rubio-Ruiz[a,b], Francisco Franco-Montalban[a], Pasquale Amoia[c], Maria Chiara Zuccarini[d], Chiara De Simone[d], M. Encarnación Camacho[a,**], ecamacho@ugr.es, Rosa Amoroso[c,*], rosa.amoroso@unich.it, Cristina Maccallini[c]

Q1

[a]Department of Medicinal and Organic Chemistry, Faculty of Pharmacy, Campus Cartuja s/n, University of Granada, 18071, Granada, Spain

[b]GENYO, Centre for Genomics and Oncological Research, Pfizer/University of Granada/Andalusian Regional Government, PTS Granada, Avda. Ilustración 114, 18016, Granada, Spain

[c]Department of Pharmacy, University "G. d'Annunzio" of Chieti-Pescara, Via dei Vestini 31, 66100, Chieti, Italy

[d]Department of Medical, Oral and Biotechnological Sciences, University "G. d'Annunzio" of Chieti-Pescara, Via dei Vestini 31, 66100, Chieti, Italy

Q2

*Corresponding author.

**Corresponding author.

Abstract

Triple negative breast cancer (TNBC) is a specific breast cancer subtype, and poor prognosis is associated to this tumour when it is in the metastatic form. The overexpression of the inducible Nitric Oxide Synthase (iNOS) is considered a predictor of poor outcome in TNBC patients, and this enzyme is reported as a valuable molecular target to compromise TNBC progression. In this work, new amidines containing a benzenesulfonamide group were designed and synthesized as selective iNOS inhibitors. An *in vitro* biological evaluation was performed to assess compounds activity against both the inducible and constitutive NOSs. The most interesting compounds **1b** and **2b** were evaluated on MDA-MB-231 cells as antiproliferative agents, and **1b** capability to counteract cell migration was also studied. Finally, an in-depth docking study was performed to shed light on the observed potency and selectivity of action of the most promising compounds.

Keywords:

Nitric oxide synthase inhibitors, Amidines, Anticancer, Benzensulfonamides, Docking, Synthesis

Abbreviations

No keyword abbreviations are available

Data availability

No data was used for the research described in the article.

1 Introduction

Breast cancer (BC) is the most prevalent cancer in females worldwide. In 2020, 2.3 million women were diagnosed with BC and 685000 deaths were recorded [1], which represents a public health issue. Among the BC subtypes, the hormone receptor (HR) positive is the most common one, followed by the human epidermal growth factor receptor 2 (HER2) positive and the so-called triple negative (TN). Based on the specific subtype, the 5-year survival to not metastatic BC can spread from 85% for the TNBC to 99% for the HR positive cancer. These percentages are dramatically lower for the metastatic disease, since the overall survival spreads from 4 to 5 years in HR and HER2 positive patients to about 1 year for the TN subgroup [2]. Considering these alarming data, it is necessary to support early screening for patients and provide new therapeutic options.

Nitric oxide (NO) is a small biomolecule which exerts multiple effects on tumor biology [3]. In general, based on the tumor micro-environment and on its concentration, NO can affect cell proliferation, migration and apoptosis [4,5]. This free radical is biosynthesized by Nitric Oxide Synthase (NOS), an oxido-reductase which is responsible for the conversion of L-arginine into L-citrulline and NO in the presence of oxygen, nicotinamide adenine dinucleotide phosphate (NADPH) and other cofactors. There are two constitutive NOS isoforms: the endothelial and the neuronal NOS (eNOS and nNOS, respectively); the eNOS plays essential roles in the vascular homeostasis, and its uncoupling is associated with the development of cardiovascular diseases [6], while the nNOS is mainly implicated in synaptic plasticity, learning and memory, and in smooth muscle relaxation [7]. Besides the constitutive NOS isoforms, there is also an inducible NOS isoform (iNOS), which is expressed in response to pro-inflammatory stimuli and, therefore, is essential in the immune system. However, iNOS can be overexpressed in many disease conditions with uncontrolled generation of NO, such as in the inflammatory bowel disease, rheumatoid arthritis, psoriasis, amyotrophic lateral sclerosis, and cancer; therefore, the inhibition of iNOS could represent a therapeutic strategy for these pathologies [8,9].

In general, the iNOS overexpression is considered a predictor of poor outcome in TNBC patients, being associated with decreased relapse-free survival [10], and different potential TNBC therapeutic targets can be modulated by iNOS [11]. It was reported that the iNOS inhibition by means of **L-NAME** and **1400W** (Fig. 1) suppressed TNBC proliferation and migration both *in vitro* and *in vivo*, impairing the EMT transcription factors, HIF1α and the reticulum stress/TGFβ/AFT4/ATF3 crosstalk [12]. Moreover, iNOS modulates the EGFR/MAPK pathway, regulating tumor progression in a pro-inflammatory environment [13]. From the clinical viewpoint, promising results were obtained from a phase 1/2 clinical trial combining the pan-NOS inhibitor **L-NMMA** with taxane in patients with chemorefractory, locally advanced breast cancer and TNBC [14]. At the same time, however, it should be noted that both **L-NAME** and **1400W** are usually used in TNBC models at very high doses, typically in the mM range [12], and that **1400W** has never passed clinical trials due to its acute toxicity.

Images are optimised for fast web viewing. Click on the image to view the original version.

alt-text: Fig. 1

Fig. 1

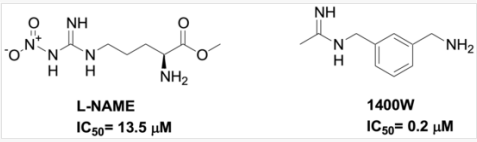

Chemical structure of iNOS inhibitors able to impair TNBC development.

Therefore, the development of safer iNOS inhibitors with ameliorated pharmacokinetic properties is desirable in order to have new valuable therapeutic tools to manage TNBC. A major problem in this regard is the lack of proper isoform and tissue selectivity for a given iNOS inhibitor. The design of selective compounds is a challenging problem because the active sites of the three NOS isozymes are highly conserved. However, modelling studies have highlighted some structural differences in the NOS active sites, mainly in the substrate access channel, and they can be exploited by introducing lipophilic and ionizable moieties in the ligand structure [15,16]. Very interestingly, an anchored plasticity approach has revealed an iNOS-specific pocket which is accessible upon conformational changes of flexible residues [17]. The introduction of rigid bulky groups in the ligand structure that extend to this specific pocket could finally result in isoform-selectivity gain [17].

In past years we have already disclosed different compounds directed against the NOS, highlighting the acetamidines **CM544** [18] and **FAB1020** [16] (Fig. 2) that showed anticancer, immunomodulatory, pro regenerative and neuroprotective activities [19–21]. Despite their potency of action against the iNOS and their improved biological profile with respect to **1400W**, these compounds are still very polar and require to be used at high doses.

Images are optimised for fast web viewing. Click on the image to view the original version.

alt-text: Fig. 2

Fig. 2

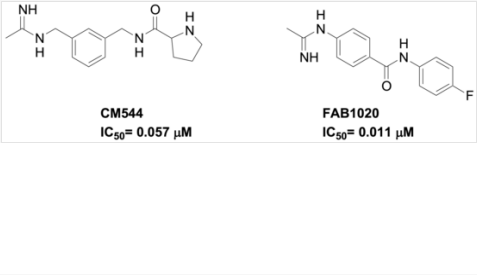

Chemical structure of iNOS inhibitors with improved potency of action.

Considering the mentioned possibility to exploit the differences between the NOSs active sites by introducing appropriate moieties and based on the results of **W1400** in the treatment of TNBC, in the present work we decided to modify its leading structure to obtain more lipophilic and bulky potential iNOS inhibitors (Fig. 3). To these aims, the acetamidine moiety was replaced by a benzamidine one, and the primary amine was linked to a benzenesulfonamide group. The latter is a well-established pharmacophoric element [22,23], and it was selected considering that the introduction of both lipophilic and ionizable groups in the structure of a potential iNOS inhibitor, can increase its potency and selectivity with respect to the constitutive isoforms [16]. A first set of compounds was prepared by linking a 4-methyl- or 4-nitro-benzenesulfonyl group to the primary amine of the **1400W** and replacing its acetamidine moiety by a substituted benzamidine one (**1a-g**). A second small set of molecules in which the 4-nitro-benzenesulfonamide moiety was connected to the *para* position of the *N*-benzylacetamidine (**2a**) or of a substituted *N*-benzylbenzamidine (**2b-d**), were synthesized in order to evaluate potential improvements in the biological activity.

Images are optimised for fast web viewing. Click on the image to view the original version.

alt-text: Fig. 3

Fig. 3

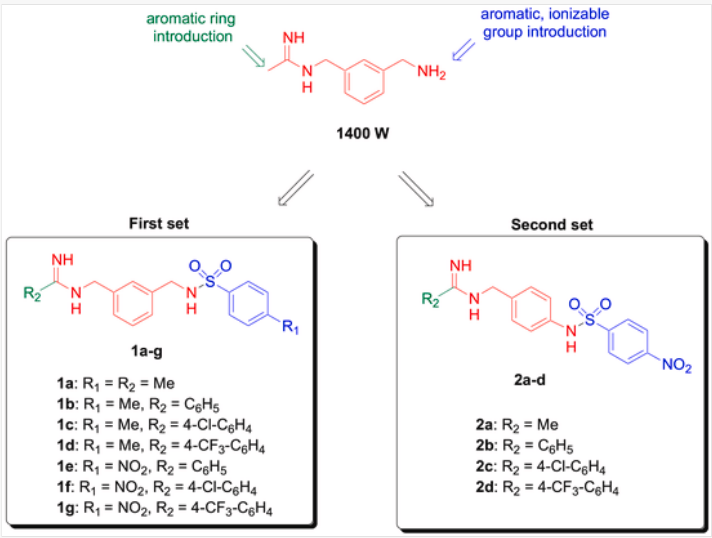

Chemical structure of the designed compounds.

The most active iNOS inhibitors **1b** and **2b** were further investigated as agents able to impair TNBC proliferation and migration with selectivity over non tumoral cells. Additionally, a computational study was performed to shed light on their binding mode into both iNOS and eNOS active sites. Finally, a microsomal stability assay was carried out on **1b** in order to predict its bioavailability.

2 Results and discussion

2.1 Chemistry

Syntheses started with the preparation of the benzimidothioates **3b-d** (Scheme 1), which was carried out in refluxing CH_2Cl_2. These compounds were then used for the preparation of the desired final compounds.

Images are optimised for fast web viewing. Click on the image to view the original version.

alt-text: Scheme 1

Scheme 1

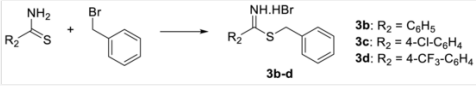

Synthesis of benzimidothioates **3b-d**. Reagents and conditions: CH_2Cl_2, reflux, 2 h.

Compounds **1a-g** were synthesized as reported in Scheme 2. The *m*-xylylenediamine was mono Boc-protected by means of the di-*t*-butyl-dicarbonate, and the resulting compound **4** was reacted with 4-methyl or 4-nitro-benzensulfonyl chloride, giving the intermediates **5a-b**, respectively, in high yields. These compounds were then deprotected in standard acidic conditions, obtaining the free base compounds **6a-b** that were finally combined with the commercial ethyl acetimidate **3a** or the benzimidothioates **3b-d,** affording **1a-g**.

Images are optimised for fast web viewing. Click on the image to view the original version.

alt-text: Scheme 2

Scheme 2

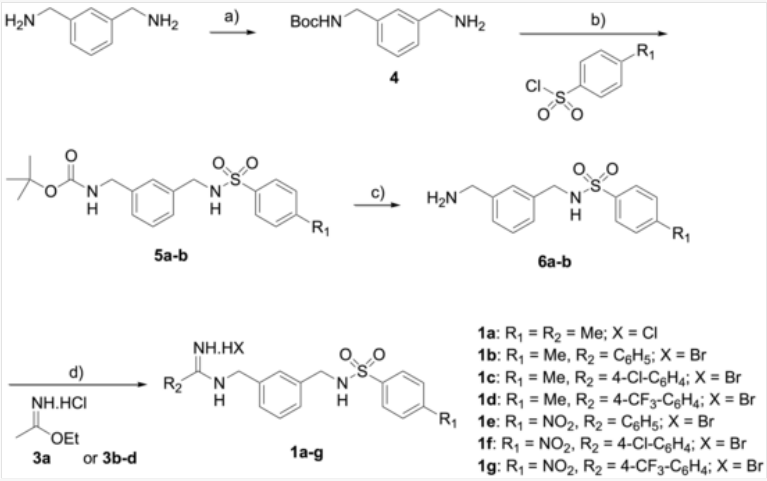

Synthetic route of novel derivatives **1a-g**. Reagents and conditions: a) Boc_2O, CH_2Cl_2, 0 °C, then room temperature (r.t.), 24 h; b) 4-methyl- or 4-nitro-benzenesulfonyl chloride, triethylamine (TEA), 0 °C, then r.t., 24 h; c) trifluoroacetic acid (TFA), CH_2Cl_2, 0 °C, 24 h; d) EtOH, r.t., 24 h.

Molecules **2a-d** were prepared following Scheme 3, starting from the selective protection of the 4-aminomethyl group of 4-aminomethylaniline with di-*t*-butyl-dicarbonate to obtain the intermediate **7**, using the same conditions as those reported for **4**. Next, compound **7** was reacted with *p*-nitrobenzenesulfonyl chloride and the obtained sulfonamide **8** was subsequently deprotected in acidic conditions, and finally condensed with the ethyl acetimidate **3a** or the benzimidothioates **3b-d**.

Images are optimised for fast web viewing. Click on the image to view the original version.

alt-text: Scheme 3

Scheme 3

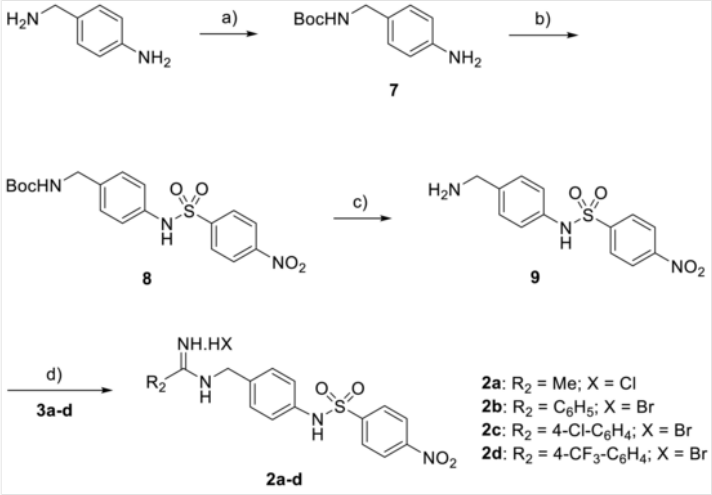

Synthetic route of novel derivatives **2a-d**. Reagents and conditions: a) Boc_2O, CH_2Cl_2, TEA, 0 °C, then r.t., 24 h; b) 4-nitrobenzenesulfonyl chloride, TEA, 0 °C, then r.t., 24 h; c) TFA, CH_2Cl_2, 0 °C, 24 h; d) EtOH, r.t., 24 h.

2.2 Nitric Oxide Synthase inhibition

All the synthesized compounds were evaluated as iNOS inhibitors, by using the L-citrulline assay with fluorimetric detection. Compounds were evaluated at 1 μM against the iNOS, and at 10 μM against the eNOS, in order to determine their isoform selectivity. Indeed, this last constitutive enzyme plays essential role in the cardiovasculature, and its inhibition must be avoided. The obtained results were expressed as enzyme percent inhibition normalized to **1400W** as the reference compound (positive control, 100% inhibition at 10 μM) and are reported in Table 1.

alt-text: Table 1

Table 1

The table layout displayed in this section is not how it will appear in the final version. The representation below is solely purposed for providing corrections to the table. To preview the actual presentation of the table, please view the Proof.

iNOS and eNOS inhibition by compounds **1a-g** and **2a-d**. Results are expressed as enzyme percent inhibition.

Compound	Inhibition (%)[a]	
	iNOS[b]	eNOS[c]
1a	n.a.	n.a.
1b	83 ± 3	n.a.
1c	72 ± 2	18 ± 2
1d	59 ± 2	28 ± 2
1e	71 ± 4	35 ± 3
1f	65 ± 3	19 ± 4
1g	72 ± 3	26 ± 2
2a	n.a.	n.a.
2b	52 ± 4	n.a.
2c	69 ± 3	46 ± 43
2d	n.a.	n.a.

Table Footnotes

[a] Values given are mean ± SD of three experiments.

[b] Evaluated in the presence of 1 μM concentration of each compound.

[c] Evaluated in the presence of 10 μM concentration of each compound. n.a. = not active.

As for the first family of amidines, compounds **1b-g** were all good inhibitors of the iNOS, with enzyme percent inhibition ranging from 59% (**1d**) to 83% (**1b**). In addition, a moderate eNOS inhibition was observed, except for **1b** which was completely inactive against this isoform. Interestingly, its corresponding acetamidine **1a** did not inhibit both the NOS isoforms. Moreover, it was observed that compounds bearing the *p*-nitro-benzamidine, i.e. **1e-g**, while retaining a good inhibition of iNOS, were more active against eNOS, compared to their methylated analogues **1b-d**. Some interesting results were obtained also from compounds **2b-d**, with a slight decrease in the inhibition of iNOS with respect to the first family of amidines (per cent inhibition were 0%, 52%, and 69%, respectively for compounds **2a**, **2b** and **2c**). However, molecule **2b** resulted a quite selective iNOS inhibitor with respect to eNOS, while its corresponding acetamidine **2a** was completely inactive.

Based on these data, compounds **1b** and **2b** were selected for biological evaluations, and their IC_{50} were at first evaluated (Table 2). Interestingly, **1b** shows an IC_{50} value against iNOS of 0.065 μM, which is very close to that of **1400W** (0.081 μM), and an excellent isoform selectivity with respect to eNOS. Although less potent with respect to the reference compound, also **2b** confirmed its potency against iNOS, while resulting inactive against eNOS. Considering their inhibition potency, both **1b** and **2b** were further investigated.

alt-text: Table 2

Table 2

The table layout displayed in this section is not how it will appear in the final version. The representation below is solely purposed for providing corrections to the table. To preview the actual presentation of the table, please view the Proof.

Inhibition of iNOS and eNOS by compounds **1b** and **2b**: IC_{50} evaluation.

Compound	IC_{50} (μM)[a]		eNOS/iNOS selectivity
	iNOS	eNOS	
1b	0.065 ± 0.003	>50	>770
2b	0.832 ± 0.025	>50	>60
1400W	0.081 ± 0.02	>50	>617

Table Footnotes

[a] Values given are mean ± SD of experiments performed in triplicate at seven different concentrations.

2.3 1b TNBC antiproliferative effects and selectivity evaluation

Based on the potential role that iNOS plays in TNBC tumor biology, we next evaluated the antiproliferative activity of compounds **1b** and **2b** in a TNBC cell line, using reference compound **1400W** as control. MDA-MB-231 cells were treated with increasing concentrations of iNOS inhibitors (0.001–100 μM) and cell viability was determined at day 5 using PrestoBlue reagent. EC_{50} values were calculated from the generated 10-point semilog concentration-response curves. As shown in Fig. 4, no reduction in cell viability was observed after treatment with compound **2b** up to 100 μM. Interestingly, compound **1b**, that proved higher potency and selectivity than **2b**, exhibited greater antiproliferative activity with an EC_{50} value of 24.71 μM. On the other hand, compound **1b** turned out to be 4-fold more active as antiproliferative agent than iNOS inhibitor **1400W** which presented an EC_{50} value > 100 μM in this assay. These findings demonstrate that the chemical modifications carried out in **1400W** structure to obtain compound **1b** have improved dramatically the therapeutic effect of **1400W**.

Images are optimised for fast web viewing. Click on the image to view the original version.

alt-text: Fig. 4

Fig. 4

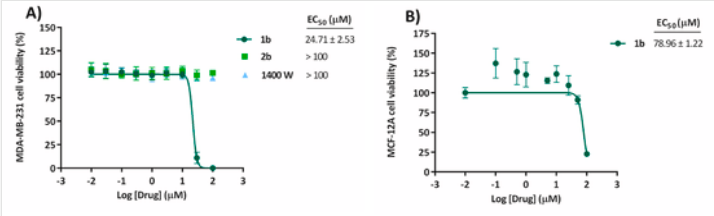

Antiproliferative activity. A): Concentration-response curves and calculated EC_{50} values for **1b**, **2b** and **1400 W** against MDA-MB-231 cells after 5 days of treatment. Error bars: ±SD from n = 3. B): Concentration -response curve of **1b** in MCF-12A cells after 5 days of treatment. Error bars: ±SD from n = 3.

In order to investigate whether compound **1b** had an anti-proliferative effect selectively on breast cancer cells, we performed the same experiment on breast non-tumoral MCF-12A cell line. Cells were treated with increasing concentrations of **1b** (0.001–100 μM) and cell viability was determined at day 5 by using PrestoBlue reagent. Untreated cells (0.1% v/v DMSO) were used as control. As shown in Figure 4, 5-day treatment with compound **1b** moderately elicited a reduction in cell viability, and the calculated EC_{50} was 78.96 μM, with a 3-fold selectivity ratio with respect to the MDA-MB-231 cells. Interestingly, MCF-12A viability was not impaired at 25 μM treatment, while only a slight decrease in cells proliferation was observed at 50 μM, being reduced to 91%.

2.4 Wound healing assay

To assess whether compound **1b** could prevent migration of TNBC cells, we performed a scratch-wound healing assay. Once the wound was made, MDA-MB-231 cells were treated with **1b** for 24 h and compared with untreated cells (0.1% v/v DMSO). Fig. 5A shows that treatment with compound **1b** reduced cell motility. Particularly, the percentage of wound closure was 15% lower in TNBC cells treated with **1b** than untreated cells (Fig. 5B). This result is consistent with previous studies that support that selective iNOS inhibition efficiently decreases migration of TNBC cell line [12].

Images are optimised for fast web viewing. Click on the image to view the original version.

alt-text: Fig. 5

Fig. 5

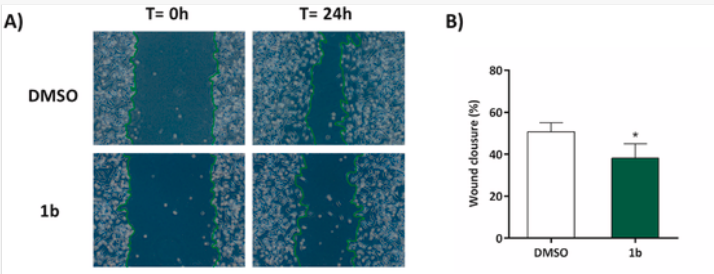

Migration assay. (A) Snapshots of the scratch-wound area of MDA-MB-231 cells treated with DMSO and **1b** at time zero (left) and after 24 h (right). Green lines highlight the gap created by the scratch. (B) Bar graph showing the percentage of wound closure of MDA-MB-231 cells after treatment with **1b** compared to untreated cell control (DMSO). Error bars: ±SD from n = 3; $p \leq 0.05$, * (ANOVA).

2.5 1b Microsomal stability evaluation

Some druglikeness, bioavailability and toxicity parameters of **1b** were predicted by means of the SwissADME on line tool (see Supporting Information), and a quite encouraging pharmacokinetic profile emerged. Moreover, **1b** toxicity prediction on CYP1A2 and CYP2C19 enzymes showed that the compound is not a substrate of these enzymes, although an in depth evaluation should be performed. To confirm **1b** metabolic stability, the evaluation of its stability in liver microsomes was carried out according to a literature method [24]. Based on the obtained data, the compound shows a reasonably metabolic stability, with a $t_{1/2}$ of 38 min and an intermediate *in vivo* intrinsic (hepatic) clearance (CL_{int}) of 39,6 mL/min Kg^{-1}. These preliminary data warrant further preclinical investigation of **1b** in a TNBC model.

2.6 Docking study

Compounds **1b** and **2b** were selected for docking studies based on their IC_{50} values and observed isoform selectivity. PDB IDs 4CX7 and 6AV7, corresponding to human iNOS and eNOS, respectively, were chosen as candidates to assess the molecular interactions of both compounds. Docking of compound **1400W** was carried out first as a positive control on both human NOS isoforms. The obtained binding poses in both proteins match those observed on published

crystal structures (see Fig. S3 in S.I.). Ligands **1b** and **2b** were studied next, and their preferred binding poses on hiNOS (PDB ID 4CX7) are shown on Fig. 6A. In both ligands, the amidine moiety mimics the guanidinium group of the natural substrate L-arginine, stablishing bidentate H-bonds with Glu377 residue and stacking interactions with the heme cofactor. However, a difference in the interplanar angle between the inhibitor phenyl ring and heme appears (5° for **1b** and 35° for **2b**), suggesting a better stacking on **1b**. As for the rest of the molecule, both inhibitors display their *p*-substituted phenyl rings toward the arginine pocket, although **2b** tilts it slightly toward the heme cofactor. Moreover, in **1b** the benzyl ring forms a stacking interaction with Tyr373, while in **2b** it sits away from Tyr373 and toward Gln263, with whom it forms a stacking interaction. On the other hand, the *p*-methyl-substituted phenylsulfonimide tail of **1b** is H-bonding Asp382 and establishing a cation-stacking interaction with Arg388, while the *p*-nitrophenyl ring of **2b** is placed in between Arg381 and the heme propionate A.

Images are optimised for fast web viewing. Click on the image to view the original version.

alt-text: Fig. 6

Fig. 6

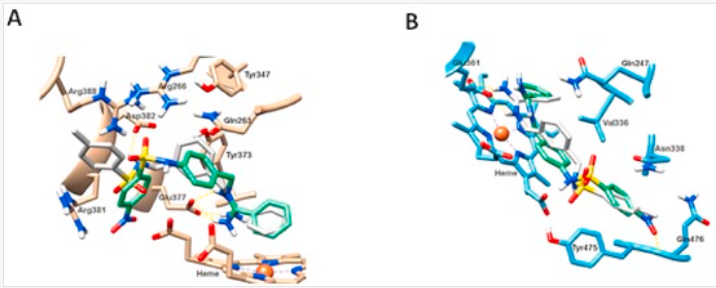

Superposition of predicted binding poses of **1b** (white) and **2b** (green) on human iNOS (PDB ID 4CX7, tan. 5A) and human eNOS (pdb ID 6AV7, blue. 5B). Hydrogen bonds are represented by dashed yellow lines.

Q3

On human eNOS (PDB ID 6AV7), a different interaction pattern can be seen for inhibitors **1b** and **2b** (Fig. 6B). Here, both compounds display their amidine group toward Glu361, but only **1b** can establish bidentate H-bonds with Glu361 although not in a coplanar orientation. Therefore, the inhibitor loses its capacity to properly H-bond Glu361 undermining the stability of the complex.

An isozyme-specific pocket has been described on iNOS. This pocket results from conformational changes of conserved first-shell (Gln263, Arg266) and second-shell (Asn283) residues upon inhibitor binding, and are in the end allowed by the less bulky, and iNOS isozyme specific, third-shell residues Val305 and Phe286 [25]. The opening and closing of this pocket is ultimately determined by the movement of Arg266 and Gln263, the former an essential residue that participates, together with Tyr373 and Glu377, in the binding of the natural substrate L-arginine [26]. Our docking results on iNOS show that both inhibitors **1b** and **2b** take advantage of the open-pocket conformation, inserting their middle phenyl ring in this cavity and allowing inhibitor **1b** to form an extra H-bond, through its sulfonimide moiety, with the iNOS-specific Asp382 (Fig. 7). This interaction might support its high selectivity toward iNOS and the nM IC_{50} value showed on *in vitro* assays. On eNOS, however, this pocket is closed, forcing the inhibitors middle phenyl ring and tails to pose underneath the heme cofactor and toward the opposite side of the catalytic site entrance, disrupting the effectiveness of the benzamidine binding on the catalytic site and supporting their low eNOS selectivity.

Images are optimised for fast web viewing. Click on the image to view the original version.

alt-text: Fig. 7

Fig. 7

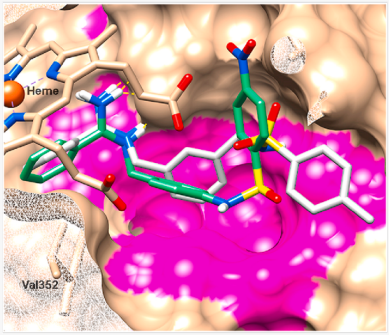

Surface representation of the docking pose of inhibitors **1b** (white) and **2b** (green) on the open conformation of human iNOS isozyme (PDB ID 4CX7). Pocket surface is colored in purple. H-bonds are represented by dashed yellow lines.

Moreover, a 10 ns molecular dynamic simulation was also carried out on the docked pose of **1b** on iNOS, and their results further sustain its stability and specificity toward this isozyme. In particular, this simulation demonstrates the stability of the amidine-Glu377 and sulfonamide-Asp382 H-bonds seen in the docked pose, and the generation of a new H-bond interaction between the amidine and the carbonyl group in the backbone chain of Trp372 (see Fig. S5 in Supporting Info). This interaction, not initially present in the docking pose of **1b** on iNOS, is characteristic when the natural substrate, L-arginine, binds the catalytic site of NOS enzymes, hence supporting the predicted binding pose of **1b** on iNOS and its selectivity toward this isoform (see Supporting Info for more details).

3 Conclusion

The inhibition of iNOS is considered a promising approach to ameliorate the standard chemotherapy of patients with TNBC, and although many different iNOS inhibitors with excellent selectivity profile were reported to date [17], no clinically approved iNOS inhibitor is currently available. Therefore, it appears urgent to find new candidates directed against the iNOS and develop them for the TNBC therapy. In the present work, we make a significant contribution to this field, reporting the design and synthesis of new amidines bearing a benzenesulfonyl moiety able to inhibit the iNOS isozyme. Compound **1b** emerged as the most interesting compound, since it is a potent and selective iNOS inhibitor (IC_{50} = 0.065 μM), and a promising antiproliferative agent against the TNBC cell line MDA-MB-231 (EC_{50} = 24.71 μM). Noteworthy, at this concentration **1b** had no effect on non-tumoral cells MCF-12A, thus revealing the promising tumor-cell specificity of this compound. Moreover, this compound compromises the MDA-MB-231 cells migration, and therefore it could be able to inhibit the TNBC invasiveness. Compared to the **1400W** activity against TNBC, a general and significant improved was obtained, in terms of potency of action of **1b** with respect to the reference compound. The performed docking study sheds light on the binding mode of the new amidines into the iNOS and eNOS catalytic sites and suggests that **1b** is a stable and specific iNOS isoform inhibitor. Moreover, **1b** shows good predicted pharmacokinetic properties (Supporting information, Table S1) with no presumable Central Nervous System side effects and displays a reasonable metabolic stability, although an in-depth evaluation by means of qualitative nucleophile trapping assays is necessary to establish if toxic metabolites are generated. In light of the collected results, **1b** can be considered a candidate for the pre-clinical development and a valuable potential agent for the therapy of TNBC.

4 Experimental

4.1 Chemistry

4.1.1 General methods and materials

All starting materials, reagents and solvents, were commercially available. ^{1}H NMR and ^{13}C NMR spectra were obtained using Bruker Avance NEO spectrometers with Smart Probe BBFO equipped, operating at 400.57 MHz for ^{1}H and 100.73 MHz for ^{13}C, in the deuterated solvents. Chemical shifts are reported in ppm (δ ppm) and are referenced to the residual solvent peak. HRMS was conducted on a Waters LCT Premier Mass Spectrometer. Melting points were determined on an electrothermal melting point apparatus and were uncorrected.

4.1.2 Synthesis of tert-butyl (3-(3-aminomethyl)benzyl)carbamate 4 [18]

A solution of di-*tert*-butyl dicarbonate (13.7 mmol) in DCM (45 mL) was added dropwise to a solution of 1,3-phenylenedimethanamine (55 mmol) in DCM (30 mL) cooled to 0 °C. Afterward, the reaction mixture was warmed to r.t. and stirred overnight. The crude was filtered and the filtrate was evaporated under reduced pressure. The residue obtained was then solubilized in AcOEt (20 mL) and washed with brine (3 × 20 mL), dried over anhydrous Na_2SO_4, filtered and evaporated. Finally, the crude was purified by flash chromatography (CH_2Cl_2/MeOH 9:1) saturated with NH_4OH. The compound was obtained as a pale yellow oil; 69% yield.

4.1.3 Synthesis of tert-butyl (3-aminobenzyl)carbamate 7 [27]

A solution of di-*t*-butyl dicarbonate (19.6 mmol) in CH_2Cl_2 (30 mL) was added dropwise to a cooled (0 °C) solution of 4-aminobenzylamine (19.6 mol) in CH_2Cl_2 (35 mL) and TEA (39.3 mmol). After the addition, the reaction mixture was warmed to r.t. and stirred overnight. It was subsequently washed with saturated NH_4Cl solution (3 × 30 mL), dried over anhydrous Na_2SO_4, filtered and evaporated. The crude was used without further purification. Orange solid; 98% yield.

4.1.4 General method for the synthesis of the Boc-protected sulfonamide intermediates 5a-b and 8

A solution of *p*-toluenesulfonyl chloride or *p*-nitrobenzenesulfonyl chloride (9.5 mmol) in DCM (17 mL) cooled to 0 °C, was added dropwise to a solution of the amine **4** or **7** (8.6 mmol) and TEA (17.2 mmol) in CH_2Cl_2 (85 mL), under magnetic stirring. After the addition, the reaction mixture was warmed to r.t. and stirred for 24 h. The crude was then washed with 5% $NaHCO_3$ solution (2 × 80 mL) and with brine (80 mL), dried over anhydrous Na_2SO_4, filtered and evaporated. The residue obtained was purified by flash chromatography or recrystallization.

Tert-butyl (3-(((4-methylphenyl)sulfonamido)methyl)benzyl)carbamate ***5a***. Purification by flash chromatography (hexane/AcOEt 7:3). Colorless solid; 83% yield. ^{1}H NMR (400 MHz, $CDCl_3$): δ 1.47 (s, 9H), 2.45 (s, 3H), 4.12 (s, 2H), 4.23 (s, 2H), 4.84 (bs, 1H), 4.94 (bs, 1H), 7.10–7.13 (m, 2H), 7.18 (dt, 1H, J = 1.5 Hz, J = 7.7 Hz), 7.25 (t, 1H, J = 7.5 Hz), 7.32 (d, 2H, J = 8.0 Hz), 7.76 (d, 2H, J = 8.3 Hz). ^{13}C NMR (100 MHz, $CDCl_3$): δ 21.54, 28.41, 44.41, 47.16, 79.68, 126.86, 126.95, 127.21, 128.97, 129.74, 136.72, 136.93, 139.50, 143.53, 155.89. HRMS (ESI): *m/z* calcd for $C_{20}H_{26}N_2O_4NaS$ $[M+Na]^+$: 413.1511; found 413.1531.

Tert-butyl (3-(((4-nitrophenyl)sulfonamido)methyl)benzyl)carbamate ***5b***. Purification by recrystallization with MeOH. White solid; 85% yield. ^{1}H NMR (400 MHz, DMSO-d_6): δ 1.40 (s, 9H), 3.18 (d, 2H, J = 4.7 Hz), 4.05 (s, 2H), 7.04–7.09 (m, 3H), 7.18 (t, 1H, J = 7.5 Hz), 7.37 (t, 1H, J = 6.2 Hz), 7.98 (d, 2H, J = 8.5 Hz), 8.35 (d, 2H, J = 8.8 Hz), 8.54 (s, 1H). ^{13}C NMR (100 MHz, DMSO-d_6): δ 28.72, 43.69, 46.73, 78.28, 124.86, 126.28, 126.54, 126.78, 128.51, 128.67, 137.44, 140.74, 146.90, 149.86, 156.25. HRMS (ESI): *m/z* calcd for $C_{19}H_{23}N_3O_6NaS$ $[M+Na]^+$: 444.1205; found 444.1205.

Tert-butyl (4-((4-nitrophenyl)sulfonamido)benzyl)carbamate ***8***. Purification by flash chromatography (DCM/AcOEt, 9:1). Yellow solid; 80% yied. ^{1}H NMR (400 MHz, $CDCl_3$): δ 1.47 (s, 9H), 4.27 (s, 2H), 4.90 (bs, 1H), 7.04 (d, 2H, J = 8.0 Hz), 7.18 (d, 2H, J = 8.0 Hz), 7.94 (d, 2H, J = 8.5 Hz), 8.29 (d, 2H, J = 8.5 Hz). ^{13}C NMR (100 MHz, $CDCl_3$): δ 28.40, 43.91, 79.90, 122.64, 124.28, 128.45, 128.52, 134.52, 137.30, 144.80, 150.23, 156.02. HRMS (ESI): *m/z* calcd for $C_{18}H_{20}N_3O_6S$ $[M-H]^-$: 406.1073; found 406.1061.

4.1.5 General method for the synthesis of the amines 6a-b and 9

TFA (58.8 mmol) was added at 0 °C to a solution in CH_2Cl_2 (36 mL) of the suitable Boc-protected sulfonamide intermediate **5a-b** or **8** (5.9 mmol) and the resulting reaction mixture was stirred overnight at r. t. Afterward, the crude was basified with 40% NaOH to pH = 14 and left under stirring for another 30 min at r.t. The aqueous phase was then separated from the organic phase and extracted with CH_2Cl_2 (2 × 15 mL). The combined organic phases were finally washed with brine (50 mL), dried over anhydrous Na_2SO_4, filtered and evaporated. The residue was purified through the procedure described below.

N-(3-(aminomethyl)benzyl)-4-methylbenzenesulfonamide ***6a***. Purification by flash chromatography (CH_2Cl_2/MeOH 9:1). Colorless oil; 86% yield. ^{1}H NMR (400 MHz, $CDCl_3$): δ 2.44 (s, 3H), 3.52 (bs, 2H), 3.76 (s, 2H), 4.09 (s, 2H), 7.07–7.24 (m, 4H), 7.30 (d, 2H, J = 8.3 Hz), 7.77 (d, 2H, J = 8.3 Hz). ^{13}C NMR (100 MHz, $CDCl_3$): δ 21.53, 45.58, 47.07, 126.70, 126.92, 127.19, 128.87, 129.72, 136.94, 137.00, 141.92, 143.43. HRMS (ESI): *m/z* calcd for $C_{15}H_{19}N_2O_2S$ $[M+H]^+$: 291.1167; found 291.1173.

N-(3-(aminomethyl)benzyl)-4-nitrobenzenesulfonamide ***6b***. Purification by recrystallization with MeOH. White solid; 71% yield. ^{1}H NMR (400 MHz, DMSO-d_6): δ 3.63 (s, 2H), 4.05 (s, 2H), 7.03–7.18 (m, 4H), 8.00 (d, 2H, J = 8.2 Hz), 8.36 (d, 2H, J = 8.4 Hz). ^{13}C NMR (100 MHz, DMSO-d_6): δ 45.91, 46.82, 124.88, 126.09, 126.42, 126.88, 128.52, 128.55, 137.25, 144.61, 146.99, 149.83. HRMS (ESI): *m/z* calcd for $C_{14}H_{16}N_3O_4S$ $[M+H]^+$: 322.0862; found 322.0881.

N-(4-(aminomethyl)benzyl)-4-nitrobenzenesulfonamide ***9***. Purification by recrystallization with MeOH. Yelow solid; 77% yield. ^{1}H NMR (400 MHz, DMSO-d_6): δ 3.70 (s, 2H), 6.82 (d, 2H, J = 8.0 Hz), 7.00 (d, 2H, J = 8.0 Hz), 7.90 (d, 2H, J = 8.3 Hz), 8.21 (d, 2H, J = 8.3 Hz). ^{13}C NMR (100 MHz, DMSO-d_6): δ 43.83, 121.09, 124.03, 127.24, 127.94, 128.94, 148.04, 148.27, 153.43. HRMS (ESI): calcd for $C_{13}H_{12}N_3O_4S$ $[M-H]^+$: 306.0549; found 306.0558.

4.1.6 General method for the synthesis of the benzyl-benzimidothioates 3b-d

A solution of benzyl bromide (2.5 mmol) in CH_2Cl_2 (2 mL) was added dropwise at r.t. to a solution of the appropriate commercially available benzothioamide (benzothioamide, 4-chlorobenzothioamide, 4-(trifluoromethyl)benzothioamide)

(2.4 mmol) in DCM (5 mL). The reaction mixture was refluxed for 2 h. Subsequently, the solvent was removed under reduced pressure and the residue was purified by crystallization with Et_2O.

Benzylbenzimidothioate hydrobromide ***3b*** [28]. White solid; mp: 194–196 °C; 97% yield.

Benzyl 4-chlorobenzimidothioate hydrobromide ***3c*** [29]. White solid; mp: 182–184 °C; 95% yield.

Benzyl 4-(trifluoromethyl)benzimidothioate hydrobromide ***3d*** [30]. White solid; mp: 147–145 °C; 90% yield.

4.1.7 General method for the synthesis of the final compounds 1a-g and 2a-d

The amines **6a-b** or **9** (1.3 mmol) were dissolved in EtOH or acetone (8 mL); then, ethyl acetimidate hydrochloride **3a** or the benzimidothioates **3b-d** (1.0 mmol) were added. The mixture was stirred for 24 h at r.t. Afterward, the reaction mixture was evaporated under reduced pressure and the residue was purified by flash chromatography (CH_2Cl_2/MeOH 9:1).

N-(3-(((4-methylphenyl)sulfonamido)methyl)benzyl)acetamidine hydrochloride ***1a***. Pale yellow solid; mp: 123–125 °C; 88% yield. ^{1}H NMR (400 MHz, $(CD_3)_2CO$): δ 2.42 (s, 3H), 2.45 (s, 3H), 4.07 (d, 2H, J = 7.0 Hz), 4.66 (d, 2H, J = 6.8 Hz), 7.23–7.39 (m, 6H), 7.83 (d, 2H, J = 8.3 Hz). ^{13}C NMR (100 MHz, $(CD_3)_2CO$): δ 18.41, 20.56, 45.79, 46.57, 126.91, 127.13, 127.42, 127.79, 128.59, 129.48, 135.02, 138.25, 142.73, 164.81. HRMS (ESI): m/z calcd for $C_{17}H_{22}N_3O_2S$ $[M+H]^+$: 332.1433; found 332.1452.

N-(3-(((4-methylphenyl)sulfonamido)methyl)benzyl)benzamidine hydrobromide ***1b***. Pale yellow solid; mp: 137–140 °C; 98% yield. ^{1}H NMR (400 MHz, $(CD_3)_2CO$): δ 2.39 (s, 3H), 4.06 (s, 2H), 4.92 (s, 2H), 7.23 (d, 2H, J = 5.0 Hz), 7.35 (d, 2H, J = 7.8 Hz), 7.50–7.71 (m, 5H), 7.81 (d, 2H, J = 8.3 Hz), 8.07 (d, 2H, J = 7.2 Hz). ^{13}C NMR (100 MHz, $(CD_3)_2CO$): δ 20.57, 45.97, 46.53, 126.98, 127.12, 127.41, 127.89, 128.45, 128.58, 128.62, 129.01, 129.48, 133.71, 135.36, 138.21, 138.23, 142.80, 163.30. HRMS (ESI): m/z calcd for $C_{22}H_{24}N_3O_2S$ $[M+H]^+$: 394.1589; found 394.1544.

4-Chloro-N-(3-(((4-methylphenyl)sulfonamido)methyl)benzyl)benzamidine hydrobromide ***1c***. Pale yellow solid; mp: 180–182 °C; 71% yield. ^{1}H NMR (400 MHz, DMSO-d_6): δ 2.39 (s, 3H), 3.96 (d, 2H, J = 6.2 Hz), 4.67 (s, 2H), 7.22–7.25 (m, 1H), 7.33–7.41 (m, 5H), 7.72 (dd, 4H, J = 5.2 Hz, J = 8.3 Hz), 7.82–7.84 (m, 2H), 8.14 (t, 1H, J = 6.3 Hz). ^{13}C NMR (100 MHz, DMSO-d_6): δ 21.45, 46.10, 46.38, 126.99, 127.03, 127.24, 127.53, 128.19, 129.09, 129.47, 130.11, 130.80, 135.76, 138.19, 138.71, 138.87, 142.90, 162.95. HRMS (ESI): m/z calcd for $C_{22}H_{23}N_3O_2SCl$ $[M+H]^+$: 428.1200; found 428.1201.

N-(3-(((4-methylphenyl)sulfonamido)methyl)benzyl)-4-trifluoromethyl)benzamidine hydrobromide ***1d***. Pale yellow solid; mp: 223–225 °C; 86% yield. ^{1}H NMR (400 MHz, CD_3OD): δ 2.33 (s, 3H), 3.97 (s, 2H), 4.59 (s, 2H), 7.14–7.35 (m, 6H), 7.64 (d, 2H, J = 8.3 Hz), 7.83 (d, 2H, J = 8.5 Hz), 7.88 (d, 2H, J = 8.4 Hz). ^{13}C NMR (100 MHz, CD_3OD): δ 20.07, 46.09, 46.36, 123.52 (q, J = 272.0 Hz), 125.93 (q, J = 3.9 Hz), 126.61, 126.67, 126.80, 127.47, 128.81, 128.84, 129.38, 132.96, 134.47, 137.64, 138.87, 143.34, 163.79. HRMS (ESI): m/z calcd for $C_{23}H_{23}N_3O_2SF_3$ $[M+H]^+$: 462.1463; found 462.1474.

N-(3-(((4-nitrophenyl)sulfonamido)methyl)benzyl)benzamidine hydrobromide ***1e***. Pale yellow solid; mp: 224–226 °C; 77% yield. ^{1}H NMR (400 MHz, DMSO-d_6): δ 4.09 (s, 2H), 4.67 (s, 2H), 7.19–7.36 (m, 4H), 7.62–7.82 (m, 5H), 8.04 (d, 2H, J = 8.3 Hz), 8.38 (d, 2H, J = 8.2 Hz). ^{13}C NMR (100 MHz, DMSO-d_6): δ 45.90, 46.45, 124.97, 127.00, 127.25, 127.55, 128.57, 128.72, 129.13, 129.44, 129.49, 133.89, 136.06, 138.29, 146.81, 149.92, 163.81. HRMS (ESI): m/z calcd for $C_{21}H_{21}N_4O_4S$ $[M+H]^+$: 425.1284; found 425.1273.

4-Chloro-N-(3-(((4-nitrophenyl)sulfonamido)methyl)benzyl)benzamidine hydrobromide ***1f***. Pale yellow solid; mp: 185–187 °C; 70% yield. ^{1}H NMR (400 MHz, DMSO-d_6): δ 4.09 (s, 2H), 4.66 (s, 2H), 7.19–7.35 (m, 4H), 7.73 (d, 2H, J = 8.7 Hz), 7.83 (d, 2H, J = 8.7 Hz), 8.04 (d, 2H, J = 8.8 Hz), 8.38 (d, 2H, J = 8.9 Hz), 8.65 (bs, 1H). ^{13}C NMR (100 MHz, DMSO-d_6): δ 46.03, 46.44, 124.96, 127.09, 127.34, 127.60, 128.20, 128.57, 129.14, 129.48, 130.77, 135.84, 138.31, 138.73, 146.81, 149.92, 162.90. HRMS (ESI): m/z calcd for $C_{21}H_{20}N_4O_4SCl$ $[M+H]^+$: 459.0894; found 459.0925.

N-(3-(((4-nitrophenyl)sulfonamido)methyl)benzyl)-4-trifluoromethyl)benzamidine hydrobromide ***1g***. Pale yellow solid; mp: 168–170 °C; 77% yield. ^{1}H NMR (400 MHz, DMSO-d_6): δ 4.10 (s, 2H), 4.69 (s, 2H), 7.20–7.37 (m, 4H), 8.03–8.06 (m, 6H), 8.38 (d, 2H, J = 8.5 Hz). ^{13}C NMR (100 MHz, DMSO-d_6): δ 46.24, 46.44, 124.92 (q, J = 272.0 Hz), 124.95, 126.24 (q, J = 3.8 Hz), 127.15, 127.40, 127.61, 128.58, 129.14, 129.99, 133.54, 135.82, 138.30, 146.81, 149.92, 162.76. HRMS (ESI): m/z calcd for $C_{22}H_{20}N_4O_4SF_3$ $[M+H]^+$: 493.1157; found 493.1180.

N-(4-((4-nitrophenyl)sulfonamido)benzyl)acetamidine hydrochloride ***2a***. Pale yellow solid; mp: 145–147 °C; 86% yield. ^{1}H NMR (400 MHz, DMSO-d_6): δ 2.18 (s, 3H), 4.36 (d, 2H, J = 5.0 Hz), 7.14 (d, 2H, J = 8.2 Hz), 7.25 (d, 2H, J = 8.2 Hz), 8.03 (d, 2H, J = 8.4 Hz), 8.39 (d, 2H, J = 8.4 Hz), 8.70 (s, 1H), 9.18 (s, 1H). ^{13}C NMR (100 MHz, DMSO-d_6): δ 19.19, 45.12, 121.13, 125.16, 128.77, 129.40, 131.90, 137.14, 145.49, 150.34, 164.69. HRMS (ESI): m/z calcd for $C_{15}H_{17}N_4O_4S$ $[M+H]^+$: 349.0971; found 349.0967.

N-(4-((4-nitrophenyl)sulfonamido)benzyl)benzamidine hydrobromide ***2b***. Pale yellow solid; mp: 140–143 °C; 84% yield. ^{1}H NMR (400 MHz, DMSO-d_6): δ 4.59 (s, 2H), 7.16 (d, 2H, J = 8.3 Hz), 7.33 (d, 2H, J = 8.2 Hz), 7.59–7.77 (m, 5H), 8.04 (d, 2H, J = 8.6 Hz), 8.38 (d, 2H, J = 8.6 Hz). ^{13}C NMR (100 MHz, DMSO-d_6): δ 45.59, 121.17, 125.14, 128.71, 128.76, 129.22, 129.39, 131.94, 133.88, 137.22, 145.61, 150.31, 163.81. HRMS (ESI): *m/z* calcd for $C_{20}H_{19}N_4O_4S$ $[M+H]^+$: 411.1127; found 411.1127.

4-Chloro-N-(4-((4-nitrophenyl)sulfonamido)benzyl)benzamidine hydrobromide ***2c***. Pale yellow solid; mp: 204–206 °C; 70% yield. ^{1}H NMR (400 MHz, DMSO-d_6): δ 4.59 (s, 1H), 7.16 (d, 2H, J = 8.1 Hz), 7.35 (d, 2H, J = 8.1 Hz), 7.70 (d, 2H, J = 8.4 Hz), 7.80 (d, 2H, J = 8.2 Hz), 8.04 (d, 2H, J = 8.5 Hz), 8.38 (d, 2H, J = 8.5 hz). ^{13}C NMR (100 MHz, DMSO-d_6): δ 45.72, 121.14, 125.14, 128.13, 128.77, 129.33, 129.42, 130.78, 131.86, 137.28, 138.68, 145.57, 150.30, 162.79. HRMS (ESI): *m/z* calcd for $C_{20}H_{18}N_4O_4SCl$ $[M+H]^+$: 445.0737; found 445.0729.

N-(4-((4-nitrophenyl)sulfonamido)benzyl)-4-trifluoromethyl)benzamidine hydrobromide ***2d***. Pale yellow solid; mp: 137–139 °C; 72% yield. ^{1}H NMR (400 MHz, DMSO-d_6): δ 4.59 (s, 2H), 7.16 (d, 2H, J = 8.3 Hz), 7.35 (d, 2H, J = 8.2 Hz), 7.95–8.05 (m, 6H), 8.39 (d, 2H, J = 8.7 Hz). ^{13}C NMR (100 MHz, DMSO-d_6): δ 45.89, 121.12, 125.16, 126.22 (q, J = 3.8), 127.90 (q, J = 271.0 Hz), 128.77, 129.40, 129.99, 131.72, 133.44, 137.19, 145.52, 150.34, 162.84. HRMS (ESI): *m/z* calcd for $C_{21}H_{18}N_4O_4SF_3$ $[M+H]^+$: 479.1001; found 479.1039.

4.2 Biology

4.2.1 NOS inhibition assay

Recombinant human iNOS was purchased from Enzo Life Sciences, Inc. (New York, USA). Recombinant bovine eNOS was purchased from Cayman Chemical (Ann Arbor, USA). To measure iNOS activity, 10 μL of enzyme stock solution were added to 80 μL of 2-[4-(2-hydroxyethyl)piperazin-1-yl]ethanesulfonic acid (HEPES) buffer pH = 7.4, 100 mM, containing 0.1 mM $CaCl_2$, 1 mM D,L-dithiothreitol (DTT), 0.5 mg/mL BSA, 10 μM flavin mononucleotide (FMN), 10 μM flavin adenine dinucleotide (FAD), 30 μM tetrahydrobiopterin (BH4), 10 μg/mL calmodulin (CaM), 10 μM L-Arg. For the eNOS activity evaluation, 25 μL of the enzyme stock solution were added to 65 μL of HEPES buffer containing 2 mM $CaCl_2$ and the same cofactors cocktail used for the iNOS assay Then, 10 μL of the test compound solution or 1400 W (0.1–100 μM) were added to the enzyme assay solution, followed by pre-incubation of 15 min at 37 °C. Each reaction was initiated by the addition of 10 μL of NADPH 7.5 mM, carried out at 37 °C for 30 min, and stopped by adding 500 μL of ice-cold CH_3CN. The mixture was brought to dryness under *vacuum* and eventually stored at −20 °C, before the HPLC analysis.

4.2.2 HPLC analysis of the NOS assays

The analysis were performed according to a previously reported method [31], with minor modifications. The o-phthalaldehyde-*N*-acetylcysteine (OPA/NAC) reagent for fluorescence derivatization of the NOS reaction mixtures was prepared with the molar ratios of 1:3, reacting 5 mL of methanolic OPA solution and 20 mL of 0.2 M borate buffer containing 0.1 g of NAC for 90 min to final pH 9.3 ± 0.05. The OPA/NAC solution was stored at 4 °C and saved for no longer than seven days. 600 μL of HPLC grade water was added to the residue of the enzymatic assay and centrifuged at 6000 rpm for 20 min. The fluorescence reaction is realized stirring 190 μL of supernatant and 60 μL of OPA/NAC solution for 5 min. HPLC analyses were performed using a Waters (Milford, MA, USA) system composed of a P600 model pump, a 2996 photodiode array detector, a 2475 multi-fluorescence detector, and a 7725i model sample injector (Rheodyne, Cotati, CA, USA). Chromatograms were recorded on a Fujitsu Siemens Esprimo computer and the Empower Pro software (Waters) processed data. The analyses were performed on an XTerra MS C8 column (250 × 4.6 mm id, 5 μm particle size) (Waters), equipped with an XTerra MS C8 guard column (Waters). A column thermostat oven mod-ule Igloo-Cil (Cil Cluzeau Info Labo, France) was used. The HPLC column was eluted at a flow rate of 0.7 mL/min with linear gradients of buffers A (5% CH_3CN in 15 mM sodium borate with 0.1% v/v TFA, pH 9.4) and B (50% CH_3CN in 8 mM sodium bo-rate with 0.1% v/v TFA, pH 9.4). The solvent gradient was 0–20% B at 0–10 min, B to 25% at 10–15 min, then to 40% at 15–20 min and to 70% at 20–28 min. This composition was maintained until t = 35 min, before being reduced to the initial 0% B composition. The injection volume was 5 μL. The fluorescence intensity in the column eluate was monitored at 335 nm (excitation) and 439 nm (emission).

4.2.3 Metabolic stability

The stability of **1b** in liver microsomes was measured according to a literature method [24]. Briefly, 0.5 μL of the compound (2 mM in DMSO stock solution) was diluted with PBS (432 μL) and a 13 μL aliquot of Sprague–Dawley rat liver microsomes (Sigma-Aldrich, No. M9066) was added. The tube was vortexed at 37 °C for 5 min, then NADPH (50 μL, 10 mM in PBS stock solution) was added. The mixture was incubated at 37 °C for 60 min, and quenched by 250 μL of ice-cold CH_3CN and centrifuged at 6000 rpm for 10 min. The supernatant was then analyzed by PDA-HPLC on Atlantis dC_{18} column (250 × 4.6 mm id, 5 μm particle size) (Waters). The HPLC column was eluted at a flow of 1 mL/min using a mixture of CH_3CN and Milli-Q H_2O (70:30). The injection volume was 5 μL. The procedure was repeated at least three times, and verapamil was used as a positive control. The microsomal intrinsic clearance ($CL_{int,\ micr}$) was calculated according to the following equation:

$$CL_{int,mic}r = \frac{0.693}{t_{1/2}} \text{ x } \frac{volume\ of\ incubation\ medium}{mg\ microsomal\ protein}$$

Finally, $CL_{int,\ micr}$ was scaled to intermediate *in vivo* intrinsic (hepatic) clearance (CL_{int}), using suitable scaling factors obtained from literature [30], according to the following equation:

$$CL_{int} = CL_{int,micr} \times \frac{mg\ microsome}{gliver} \times \frac{liver\ weight\ (g)}{bodyweight\ (Kg)}$$

where 45 mg of microsomal protein per gram of liver tissue and 40 g of liver tissue per kilogram of body weight were applied [32].

4.2.4 Cell culture

Human breast carcinoma MDA-MB-231 cells (purchased from ATCC) were cultured in Dulbecco's Modified Eagle Media (DMEM) with 10% fetal bovine serum (FBS) and L-glutamine (2 mM). Human non-tumoral breast MCF-12A cells (purchased from ATCC) were grown in DMEM/F12, 1:1, 5% equine serum, 20 ng/mL EGF, 0.5 μg/mL hydrocortisone, 0.1 μg/mL cholera toxin, and 10 μg/mL insulin. Both cell lines were maintained in a tissue culture incubator at 37 °C, 5% CO_2 and 95% relative humidity. Cells were frequently tested negative for mycoplasma infection.

4.2.4.1 Cell viability study

MDA-MB-231 and MCF-12A cells were seeded in a 96-well plate (2000 cells/well) in triplicate and allowed to grow for 24 h before treating them with compounds **1b**, **2b** and **1400 W** (0.01–100 μM) for 5 days. . Untreated cells (control) were treated with DMSO (0.1% v/v). Each condition was performed in triplicates. PrestoBlue™ cell viability reagent (10% v/v) was added to each well and the plate incubated for 120 min. Fluorescence emission was detected using a GloMax-Multi Detection System (excitation filter at 540 nm and emission filter at 590 nm). All conditions were normalized to the untreated cells (100%) and curves fitted using GraphPad Prism using a sigmoidal variable slope curve. EC_{50} (half-maximal effective concentration) values are expressed as mean ± SD of 3 independent experiments.

4.2.4.2 Wound healing assay

MDA-MB-231 cells were seeded in a 12-well plate format at 20×10^4 cells/well. After 12 h of incubation, the media was replaced and cells kept in starvation conditions (1% FBS) for 24 h. Then, cells were gently scratched using a pipette tip, washed with PBS to remove cell debris and treated with **1b** (25 μM) in starvation conditions. Untreated cells (DMSO, 0.1% v/v) were used as controls. Images were acquired at time zero and after 24 h of incubation using an Olympus CKX53 microscope (4× objective magnification). Wound areas were measured using ImageJ® software.

4.3 Docking study

4.3.1 Docking protocol

Docking studies were carried out with Autodock 4.2.6 (AD4) [33] on the iNOS and eNOS isozymes (pdb IDs 4CX7 and 6AV7 respectively). Ligands structures were built on Avogadro [34] and optimized using Gaussian [33] (HF/6-31G(d,p)). Once optimized, ligands PDBs were prepared for docking using the prepare_ligand4.py script included MGLTools 1.5.4 [35]. Protein structures, on the other hand, were prepared for docking using the PDB2PQR tools [36]. Water and ligand molecules were removed and charges and non-polar hydrogen atoms were added at pH 7.0. The produced structures were saved as a pdb files and prepared for docking using the prepare_receptor4.py script from MGLTools. The Fe atom of heme was assigned a charge of +2. AD4 was used to automatically dock the ligands into the iNOS and eNOS binding sites. For both enzymes, the docking grid was centered on the ligand binding site and set with the following grid parameters: 60 Å × 60 Å × 60 Å with 0.375 Å spacing. In all calculations, AD4 parameter file was set to 100 GA runs, 2.500.000 energy evaluations and a population size of 150. The Lamarckian genetic algorithm local search (GALS) method was used for the docking calculations. All dockings were performed with a population size of 250 and a Solis and Wets local search of 300 rounds was applied with a probability of 0.06. A mutation rate of 0.02 and a crossover rate of 0.8 were used. The docking results from each of the 100 calculations were clustered based on root-mean square deviation (RMSD) solutions differing by less than 2.0 Å between the Cartesian coordinates of the atoms and ranked on the basis of free energy of binding. The obtained conformations were individually inspected using UCSF Chimera 1.15 [37]. This software was also used for figures generation.

4.3.2 Molecular dynamics (MD) protocol

The docked pose of inhibitor **1b** obtained in AD4 was fit into a model of human iNOS generated using as template a modeled pdb structure of the iNOS oxygenase domain (PDB ID 4CX7). This crystal structure is missing a loop section of 16 residues and the complete oxygenase domain was built using CHARMM-GUI online server [38] and the aforementioned pdb (4CX7) as template. The inhibitor-protein ensemble was subjected to atomistic molecular dynamic (MD) simulation on NAMD 2.14 [7]. Protein and ligands were parametrized using CHARMM force field [38–41] and the MD simulation was run using NAMD 2.14. The initial ensemble was first submitted to a 30 ps (ps) energy minimization at 300K on periodic boundary conditions to remove high-energy contacts, followed by successive 300 ps NVT and a 1 ns (ns) NPT equilibration before the productive 10 ns MD simulation. During the productive MD, water bonds were constrained using the SHAKE algorithm [42]; for every 2 fs, neighbors were searched in grid cells with 1 nm as the cutoff value for short-range neighborlist, electrostatic, and van der Waals; long-range electrostatics were treated with the particle mesh Ewald method [43] with a grid spacing of 1; constant temperature and pressure were maintained by coupling the system to an external bath at 300 K and 1 bar, using velocity rescaling [44] and Parrinello−Rahman [45], respectively. A RESPA propagator with the integration time step of 1 fs was used [46]. TIP3P model was applied for water [47], and UCSF Chimera 1.15 was used to perform the trajectory analyses and generate the final images [37].

Funds

The present work was supported by University “G. d’Annunzio” of Chieti-Pescara local grants: FAR Maccallini 2019; Q4 FAR Amoroso 2020.

Declaration of competing interest

The authors declare that they have no known competing financial interests or personal relationships that could have appeared to influence the work reported in this paper.

Acknowledgments

We thank the Centro de Servicios de Informática y Redes de Comunicaciones (CSIRC), Universidad de Granada, for providing the computing time and resources.

Appendix A Supplementary data

Supplementary data to this article can be found online at https://doi.org/10.1016/j.ejmech.2023.115112.

References

The corrections made in this section will be reviewed and approved by a journal production editor. The newly added/removed references and its citations will be reordered and rearranged by the production team.

[1] World Health Organization, Breast cancer Available online: https://www.who.int/news-room/fact-sheets/detail/breast-cancer.

[2] S. Duranti, A. Fabi, M. Filetti, R. Falcone, P. Lombardi, G. Daniele, G. Franceschini, L. Carbognin, A. Palazzo, G. Garganese, I. Paris, G. Scambia, A. Pietragalla, Breast cancer drug approvals issued by EMA: a review of clinical trials, Cancers 13 (2021) 5198, doi:10.3390/cancers13205198.

[3] A.J. Burke, F.J. Sullivan, F.J. Giles, S.A. Glynn, The yin and yang of nitric oxide in cancer progression, Carcinogenesis 34 (2013) 503–512, doi:10.1093/carcin/bgt034.

[4] S. Pervin, R. Singh, E. Hernandez, G. Wu, G. Chaudhuri, Nitric oxide in physiologic concentrations targets the translational machinery to increase the proliferation of human breast cancer cells: involvement of mammalian target of rapamycin/eIF4E pathway, Cancer Res. 67 (2007) 289–299, doi:10.1158/0008-5472.CAN-05-4623.

[5] P.J. Shami, D.L. Sauls, J.B. Weinberg, Schedule and concentration-dependent induction of apoptosis in leukemia cells by nitric oxide, Leukemia 12 (1998) 1461–1466.

[6] A.M. Pourbagher-Shahri, T. Farkhondeh, M. Talebi, D.M. Kopustinskiene, S. Samarghandian, J. Bernatoniene, An overview of NO signaling pathways in aging, Molecules 26 (2021) 4533, doi:10.3390/molecules26154533.

[7] Y. Wang, D.C. Newton, P.A. Marsden, N.O.S. Neuronal, Gene structure, mRNA diversity, and functional relevance, Crit. Rev. Neurobiol. 13 (1999) 21–43, doi:10.1615/CritRevNeurobiol.v13.i1.20.

[8] M.A. Cinelli, H.T. Do, G.P. Miley, R.B. Silverman, Inducible nitric oxide synthase: regulation, structure, and inhibition, Med. Res. Rev. 40 (2020) 158–189, doi:10.1002/med.21599.

[9] C. Maccallini, M. Gallorini, A. Cataldi, R. Amoroso, Targeting iNOS as a valuable strategy for the therapy of glioma, ChemMedChem 15 (2020) 339–344.

[10] S.A. Glynn, B.J. Boersma, T.H. Dorsey, M. Yi, H.G. Yfantis, L.A. Ridnour, et al., Increased NOS2 predicts poor survival in estrogen receptor-negative breast cancer patients, J. Clin. Invest. 120 (2010) 3843–3854, doi:10.1172/JCI42059.

[11] E.M. Walsh, M.M. Keane, D.A. Wink, G. Callagy, S.A. Glynn, Review of triple negative breast cancer and the impact of inducible Nitric Oxide Synthase on tumor biology and patient outcomes, Crit. Rev. Oncog. 21 (2016) 333–351, doi:10.1615/CritRevOncog.2017021307.

[12] S. Granados-Principal, Y. Liu, M.L. Guevara, E. Blanco, D.S. Choi, W. Qian, T. Patel, A.A. Rodriguez, J. Cusimano, H.L. Weiss, H. Zhao, M.D. Landis, B. Dave, S.S. Gross, J.C. Chang, Inhibition of iNOS as a novel effective targeted therapy against triple-negative breast cancer, Breast Cancer Res. 17 (2015) 25, doi:10.1186/s13058-015-0527-x.

[13] P. Garrido, A. Shalaby, E.M. Walsh, N. Keane, M. Webber, M. Keane, F.J. Sullivan, M.J. Kerin, G. Callagy, A.E. Ryan, S.A. Glynn, Impact of inducible nitric oxide synthase (iNOS) expression on triple negative breast cancer outcome and activation of EGFR and ERK signaling pathways, Oncotarget 8 (2017) 80568–80588, doi:10.18632/oncotarget.19631.

[14] A.W. Chung, K. Anand, A.C. Anselme, A.A. Chan, N. Gupta, L.A. Venta, M.R. Schwartz, W. Qian, Y. Xu, L. Zhang, J. Kuhn, T. Patel, A.A. Rodriguez, A. Belcheva, J. Darcourt, J. Ensor, E. Bernicker, P.Y. Pan, S.H. Chen, D.J. Lee, P.A. Niravath, J.C. Chang, A phase 1/2 clinical trial of the nitric oxide synthase inhibitor L-NMMA and taxane for treating chemoresistant triple-negative breast cancer, Sci. Transl. Med. 13 (2021) eabj5070, doi:10.1126/scitranslmed.abj5070.

[15] H. Ji, H. Li, M. Flinspach, T.L. Poulos, R.B. Silverman, Computer modeling of selective regions in the active site of nitric oxide synthases: implication for the design of isoform-selective inhibitors, J. Med. Chem. 46 (2003) 5700–5711, doi:10.1021/jm030301u.

[16] C. Maccallini, F. Arias, M. Gallorini, P. Amoia, A. Ammazzalorso, B. De Filippis, M. Fantacuzzi, L. Giampietro, A. Cataldi, M.E. Camacho, R. Amoroso, Antiglioma activity of aryl and amido-aryl acetamidine derivatives targeting iNOS: synthesis and biological evaluation, ACS Med. Chem. Lett. 11 (2020) 1470–1475, doi:10.1021/acsmedchemlett.0c00285.

[17] E.D. Garcin, A.S. Arvai, R.J. Rosenfeld, M.D. Kroeger, B.R. Crane, G. Andersson, G. Andrews, P.J. Hamley, P.R. Mallinder, D.J. Nicholls, S.A. St-Gallay, A. C Tinker, N.P. Gensmantel, A. Mete, D.R. Cheshire, S. Connolly, D.J. Stuehr, A. Aberg, A.V. Wallace, J.A. Tainer, E.D. Getzoff, Anchored plasticity opens doors for selective inhibitor design in nitric oxide synthase, Nat. Chem. Biol. 11 (2008) 700–707, doi:10.1038/nchembio.115.

[18] C. Maccallini, M. Di Matteo, M. Gallorini, M. Montagnani, V. Graziani, A. Ammazzalorso, P. Amoia, B. De Filippis, S. Di Silvestre, M. Fantacuzzi, L. Giampietro, M.A. Potenza, N. Re, A. Pandolfi, A. Cataldi, R. Amoroso, Discovery of N-{3-[(ethanimidoylamino)methyl]benzyl}-l-prolinamide dihydrochloride: a new potent and selective inhibitor of the inducible nitric oxide synthase as a promising agent for the therapy of malignant glioma, Eur. J. Med. Chem. 152 (2018) 53–64, doi:10.1016/j.ejmech.2018.04.027.

[19] M. Gallorini, C. Maccallini, A. Ammazzalorso, P. Amoia, B. De Filippis, M. Fantacuzzi, L. Giampietro, A. Cataldi, R. Amoroso, The selective acetamidine-based iNOS inhibitor CM544 reduces glioma cell proliferation by enhancing PARP-1 cleavage in vitro, Int. J. Mol. Sci. 20 (2019) 495 20.

[20] M. Gallorini, M. Rapino, H. Schweikl, A. Cataldi, R. Amoroso, C. Maccallini, Selective inhibitors of the inducible nitric oxide synthase as modulators of cell responses in LPS-stimulated human

monocytes, Molecules 26 (2021) 4419.

[21] S. Grottelli, R. Amoroso, L. Macchioni, F. D'Onofrio, K. Fettucciari, I. Bellezza, C. Maccallini, Acetamidine-based iNOS inhibitors as molecular tools to counteract inflammation in BV2 microglial cells, Molecules 25 (2020) 2646.

[22] Y. Ren, Y. Ma, S. Cherukupalli, J.E. Tavis, L. Menéndez-Arias, X. Liu, P. Zhan, Discovery and optimization of benzenesulfonamides-based hepatitis B virus capsid modulators via contemporary medicinal chemistry strategies, Eur. J. Med. Chem. 206 (2020) 112714, doi:10.1016/j.ejmech.2020.112714.

[23] S. Apaydın, M. Török, Sulfonamide derivatives as multi-target agents for complex diseases, Bioorg. Med. Chem. Lett. 29 (2019) 2042–2050, doi:10.1016/j.bmcl.2019.06.041.

[24] X. Zhang, K. Kumata, T. Yamasaki, R. Cheng, A. Hatori, L. Ma, Y. Zhang, L. Xie, L. Wang, H.J. Kang, D.J. Sheffler, N.D.P. Cosford, M.R. Zhang, S.H. Liang, Synthesis and preliminary studies of a novel negative allosteric modulator, 7-((2,5-dioxopyrrolidin-1-yl)methyl)-4-(2-fluoro-4-[11C]methoxyphenyl) quinoline-2-carboxamide, for imaging of metabotropic glutamate receptor 2, ACS Chem. Neurosci. 8 (2017) 1937–1948, doi:10.1021/acschemneuro.7b00098.

[25] E.D. Garcin, A.S. Arvai, R.J. Rosenfeld, M.D. Kroeger, B.R. Crane, G. Andersson, G. Andrews, P.J. Hamley, P.R. Mallinder, D.J. Nicholls, S.A. St-Gallay, A.C. Tinker, N.P. Gensmantel, A. Mete, D.R. Cheshire, S. Connolly, D.J. Stuehr, A. Åberg, A.V. Wallace, J.A. Tainer, E.D. Getzoff, Anchored plasticity opens doors for selective inhibitor design in nitric oxide synthase, Nat. Chem. Biol. 4 (2008) 700–707, doi:10.1038/nchembio.115.

[26] H. Li, C.S. Raman, C.B. Glaser, E. Blasko, T.A. Young, J.F. Parkinson, M. Whitlow, T.L. Poulos, Crystal structures of zinc-free and -bound heme domain of human Inducible Nitric-oxide Synthase: implications for dimer stability and comparison with endothelial nitric-oxide synthase, J. Biol. Chem. 274 (1999) 21276–21284, doi:10.1074/jbc.274.30.21276.

[27] Y. Zhu, D. Nikolic, R.B. Van Breemen, R.B. Silverman, Mechanism of inactivation of inducible Nitric Oxide Synthase by amidines. Irreversible enzyme inactivation without inactivator modification, J. Am. Chem. Soc. 127 (2005) 858–868, doi:10.1021/ja0445645.

[28] B.G. Shearer, J.A. Oplinger, S. Lee, S-2-Naphthylmethyl thioacetimidate hydrobromide: a new odorless reagent for the mild synthesis of substituted acetamidines, Tetrahedron Lett. 38 (1997) 179–182, doi:10.1016/S0040-4039(96)02268-X.

[29] L. Varoli, S. Burnelli, L. Garuti, B. Vitali, Synthesis and antimicrobial activity of new diazoimidazole derivatives containing an N-acylpyrrolidine ring, Il Farmaco 56 (2011) 885–890.

[30] F. Arias, F. Franco-Montalbán, M. Romero, M.D. Carrión, M.E. Camacho, Synthesis, bioevaluation and docking studies of new imidamide derivatives as nitric oxide synthase inhibitors, Bioorg. Med. Chem. 44 (2021) 116294, doi:10.1016/j.bmc.2021.116294.

[31] C. Maccallini, M. Gallorini, F. Sisto, A. Akdemir, A. Ammazzalorso, B. De Filippis, M. Fantacuzzi, L. Giampietro, S. Carradori, A. Cataldi, R. Amoroso, New azolyl-derivatives as multitargeting agents against breast cancer and fungal infections: synthesis, biological evaluation and docking study, J. Enzym. Inhib. Med. Chem. 36 (2021) 1632–1645, doi:10.1080/14756366.2021.1954918.

[32] K. Słoczyńska, A. Gunia-Krzyżak, P. Koczurkiewicz, K. Wójcik-Pszczoła, D. Żelaszczyk, J. Popiół, E. Pękala, Metabolic stability and its role in the discovery of new chemical entities, Acta Pharm. 69 (2019) 345–361, doi:10.2478/acph-2019-0024.

[33] G.M. Morris, R. Huey, W. Lindstrom, M.F. Sanner, R.K. Belew, D.S. Goodsell, A.J. Olson, AutoDock4 and AutoDockTools4: automated docking with selective receptor flexibility, J. Comput. Chem. 30 (2009) 2785–2791, doi:10.1002/jcc.21256.

[34] M.D. Hanwell, D.E. Curtis, D.C. Lonie, T. Vandermeersch, E. Zurek, G.R. Hutchison, Avogadro: an advanced semantic chemical editor, visualization, and analysis platform, J. Cheminf. 4 (2012) 17, doi:10.1186/1758-2946-4-17.

[35]

M.J. Frisch, G.W. Trucks, H.B. Schlegel, G.E. Scuseria, M.A. Robb, J.R. Cheeseman, G. Scalmani, V. Barone, B. Mennucci, G.A. Petersson, H. Nakatsuji, M. Caricato, X. Li, H.P. Hratchian, A.F. Izmaylov, J. Bloino, G. Zheng, J.L. Sonnenberg, M. Hada, M. Ehara, K. Toyota, R. Fukuda, J. Hasegawa, M. Ishida, T. Nakajima, Y. Honda, O. Kitao, H. Nakai, T. Vreven, J.A. Montgomery Jr., J.E. Peralta, F. Ogliaro, M. Bearpark, J.J. Heyd, E. Brothers, N. Kudin, V.N. Staroverov, T. Keit, R. Kobayashi, J. Normand, K. Raghavachari, A. Rendell, J.C. Burant, S.S. Iyengar, J. Tomasi, M. Cossi, N. Rega, J.M. Millam, M. Klene, J.E. Knox, J.B. Cross, V. Bakken, C. Adamo, J. Jaramillo, R. Gomperts, R.E. Stratmann, O. Yazyev, A.J. Austin, R. Cammi, C. Pomelli, J.W. Ochterski, L. Martin, K. Morokuma, V.G. Zakrzewski, G.A. Voth, P. Salvador, J.J. Dannenberg, S. Dapprich, A.D. Daniels, O. Farkas, J.B. Foresman, J.V. Ortiz, J. Cioslowski, D.J. Fox, GAUSSIAN 09 (Revision D.1), GAUSSIAN 09 (Revision B.01), 2010.

[36] T.J. Dolinsky, J.E. Nielsen, J.A. McCammon, N.A. Baker, PDB2PQR: an automated pipeline for the setup of Poisson–Boltzmann electrostatics calculations, Nucleic Acids Res. 32 (2004) W665–W667, doi:10.1093/nar/gkh381.

[37] E.F. Pettersen, T.D. Goddard, C.C. Huang, G.S. Couch, D.M. Greenblatt, E.C. Meng, T.E. Ferrin, UCSF Chimera - a visualization system for exploratory research and analysis, J. Comput. Chem. 25 (2004) 1605–1612, doi:10.1002/jcc.20084.

[38] S. Jo, T. Kim, V.G. Iyer, W. Im Charmm-Gui, A web-based graphical user interface for CHARMM, J. Comput. Chem. 29 (2008) 1859–1865, doi:10.1002/jcc.20945.

[39] J.C. Phillips, D.J. Hardy, J.D.C. Maia, J.E. Stone, J.V. Ribeiro, R.C. Bernardi, R. Buch, G. Fiorin, J. Hénin, W. Jiang, R. McGreevy, M.C.R. Melo, B.K. Radak, R.D. Skeel, A. Singharoy, Y. Wang, B. Roux, A. Aksimentiev, Z. Luthey-Schulten, L.V. Kalé, K. Schulten, C. Chipot, E. Tajkhorshid, Scalable molecular dynamics on CPU and GPU architectures with NAMD, J. Chem. Phys. 153 (2020) 044130, doi:10.1063/5.0014475.

[40] B.R. Brooks, C.L. Brooks III, A.D. Mackerell Jr., L. Nilsson, R.J. Petrella, B. Roux, Y. Won, G. Archontis, C. Bartels, S. Boresch, A. Caflisch, L. Caves, Q. Cui, A.R. Dinner, M. Feig, S. Fischer, J. Gao, M. Hodoscek, W. Im, K. Kuczera, T. Lazaridis, J. Ma, V. Ovchinnikov, E. Paci, R.W. Pastor, C.B. Post, J.Z. Pu, M. Schaefer, B. Tidor, R.M. Venable, H.L. Woodcock, X. Wu, W. Yang, D.M. York, M. Karplus, CHARMM: the biomolecular simulation program, J. Comput. Chem. 30 (2009) 1545–1614, doi:10.1002/jcc.21287.

[41] S. Kim, J. Lee, S. Jo, C.L. Brooks III, H.S. Lee, W. Im, CHARMM-GUI ligand reader and modeler for CHARMM force field generation of small molecules, J. Comput. Chem. 38 (2017) 1879–1886, doi:10.1002/jcc.24829.

[42] J.-P. Ryckaert, G. Ciccotti, H.J.C. Berendsen, Numerical integration of the cartesian equations of motion of a system with constraints: molecular dynamics of n-alkanes, J. Comput. Phys. 23 (1977) 327–341, doi:10.1016/0021-9991(77)90098-5.

[43] T. Darden, D. York, L. Pedersen, Particle mesh Ewald: an N·log(N) method for Ewald sums in large systems, J. Chem. Phys. 98 (1993) 10089–10092, doi:10.1063/1.464397.

[44] G. Bussi, D. Donadio, M. Parrinello, Canonical sampling through velocity rescaling, J. Chem. Phys. 126 (2007) 014101, doi:10.1063/1.2408420.

[45] M. Parrinello, A. Rahman, Polymorphic transitions in single crystals: a new molecular dynamics method, J. Appl. Phys. 52 (1981) 7182–7190, doi:10.1063/1.328693.

[46] M. Tuckerman, B.J. Berne, G.J. Martyna, Reversible multiple time scale molecular dynamics, J. Chem. Phys. 97 (1992) 1990–2001, doi:10.1063/1.463137.

[47] W.L. Jorgensen, J. Chandrasekhar, J.D. Madura, R.W. Impey, M.L. Klein, Comparison of simple potential functions for simulating liquid water, J. Chem. Phys. 79 (1983) 926–935, doi:10.1063/1.445869.

Graphical abstract

Images are optimised for fast web viewing. Click on the image to view the original version.

alt-text: Image 1

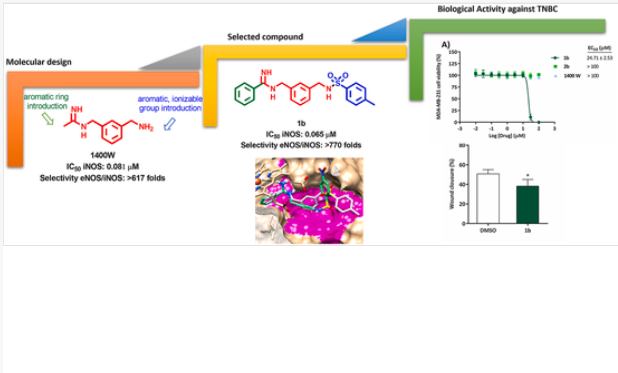

Highlights

- Novel amidine-benzenesulfonamides were designed starting from the lead compound 1400 W
- The new compounds were evaluated as iNOS inhibitors with an HPLC method with fluorimetric detection.
- Compounds **1b** showed antiproliferative action against triple negative breast cancer cells.
- Compund **1b** reduced cell motility in a scratch-wound healing assay.
- A docking study was performed to shed light on the potency and selectivity of the most promising compounds.

Appendix A Supplementary data

The following is the Supplementary data to this article.

Multimedia Component 1

Multimedia component 1

alt-text: Multimedia component 1

Queries and Answers

Q1

Query: Please confirm that the provided **emails** "rosa.amoroso@unich.it, ecamacho@ugr.es" are the correct address for official communication, else provide an alternate e-mail address to replace the existing one, because private e-mail addresses should not be used in articles as the address for communication.

Answer:

Q2

Query: Please check that the **affiliations** link the authors with their correct departments, institutions, and locations, and correct if necessary.

Answer:

Q3

Query: The following number has been identified as PDB accession number. Please verify if this is correct.

Answer:

Q4

Query: Have we correctly interpreted the following funding source(s) you cited in your article: University “G. d’Annunzio” of Chieti-Pescara local.?

Answer:

Q5

Query: Please confirm that **given names and surnames** have been identified correctly and are presented in the desired order and please carefully verify the spelling of all authors' names.

Answer:

Q6

Query: Your article is registered as a regular item and is being processed for inclusion in a regular issue of the journal. If this is NOT correct and your article belongs to a Special Issue/Collection please contact v.david@elsevier.com immediately prior to returning your corrections.

Answer: